R. F. Broom W. Kotyczka A. Moser

Modeling of Characteristics for Josephson Junctions Having Nonuniform Width or Josephson Current Density

Several models, both static and dynamic, for calculating the maximum dc Josephson current versus external magnetic field "characteristic" of tunnel junctions of various geometries are described. The static models have the advantage of short computation times; the dynamic models, although slower, yield additional information on circuit-switching times. The dependence of the characteristics on the junction shape is described. The accuracy of a one-dimensional approximation used in the models has been tested experimentally, and theoretically against a two-dimensional approximation. In both cases, the one-dimensional treatment yields quantitatively good agreement provided the inductance of the junction is included in the model. Junctions defined by an oxide "window" of sinusoidal shape (maximum and minimum width at the center and ends, respectively) have a characteristic in which the side lobes are almost completely suppressed. The characteristics of a wide variety of junction shapes, including interferometers having two or more junctions, have been accurately calculated, permitting the design of devices for specific purposes.

Introduction

The dependence of the maximum dc Josephson current on magnetic field exhibits a simple Fraunhofer diffraction pattern when the junction width W is uniform and the length ℓ is smaller than about twice the Josephson penetration length $\lambda_{\rm J}$ [1, 2]. However, for larger values of $\ell/\lambda_{\rm J}$, the self-field of the junction current has an increasing influence, and the resultant characteristic depends strongly on the geometry of the junction. Such cases cannot be solved in a simple analytical form and have been the subject of a number of theoretical [3–8] and experimental [4, 5, 7, 9] investigations. With suitably chosen junction geometry the experimental results show good agreement with one-dimensional numerical calculations.

Josephson tunnel junctions are now being studied for logic and memory applications [10-15]. With regard to "small" junctions having $\ell/\lambda_{\rm J} \le 2$, it is easily shown that the control current $i_{\rm c}$ required to reduce the dc Josephson gate current of the junction $i_{\rm l}$ to the first minimum of the Fraunhofer diffraction pattern, defined here as $i_{\rm c}(0)$, is given by $2\pi i_{\rm l}/(\ell/\lambda_{\rm J})^2$, where $i_{\rm l}$ is the Josephson current

density j_1 multiplied by the junction area A. Consequently the "current gain," defined here by the ratio $i_1/i_c(0)$, is small ($\leq \pi/2$), restricting the usefulness of such junctions. The advantages of dc isolation between input and output provided by control lines, and the higher current gain of long junctions having $\ell/\lambda_J \geq 3$ make such structures more generally suitable for circuit applications. In this respect the ability successfully to design circuits with specified properties requires an accurate knowledge of the static and dynamic characteristics of the junctions. For the static behavior, calculation of the junction current i_g versus i_c for various values of ℓ/λ_J is an important part of determining the operating regions and hence the suitability of a given set of parameters.

For a constant junction width W and current density j_1 along the length of the junction, one-dimensional models lead to a single family of curves for the characteristic i_g versus i_g . The shape of the curves depends only on the single parameter ℓ/λ_g . However, it is known that varying either j_g [16] or W [13] along the length can strongly influ-

Copyright 1980 by International Business Machines Corporation. Copying is permitted without payment of royalty provided that (1) each reproduction is done without alteration and (2) the *Journal* reference and IBM copyright notice are included on the first page. The title and abstract may be used without further permission in computer-based and other information-service systems. Permission to *republish* other excerpts should be obtained from the Editor.

ence the characteristic, especially in those regions of i_c where the junction contains one or more flux quanta Φ_0 ($\Phi_0 = h/2e \approx 2.07 \times 10^{-15}$ Wb). By these means the available range of characteristics can be extended. In principle, the former restriction of a single family of curves is lifted and the ability to "tailor" curves to best fulfill a particular purpose is greatly enhanced.

The first approach, variation of j_1 , can be realized with a structure that is uniform along the length. For appropriate geometry it can be treated as a one-dimensional problem. The calculations are relatively simple but realization of a spatially varying thickness of the tunnel barrier is very difficult to achieve in a controlled manner. The second alternative, variation of W, is technologically much easier; however, calculation of the characteristics is apparently more difficult because two dimensions must be considered for a rigorous solution.

In this paper we report the results of a number of models, mainly one-dimensional, that have been used to obtain the calculated characteristics for the two cases just mentioned.

Theory

The equations that must be solved to obtain the characteristic are well known and have been described in several publications [3–8]; thus, we summarize here only the necessary relations in their most general form.

We assume the junction to be in the x-y plane, to be of length ℓ in the x direction, and to be of width W in the y direction. The surface currents in the superconductors flow in the x-y plane only and the tunnel current between the electrodes is assumed to be restricted to the z direction. For this geometry the Josephson equations are

$$j = j_1 \sin \phi; \tag{1}$$

$$\frac{\partial \phi}{\partial x} = \frac{2ed}{\hbar} B_y, \qquad \frac{\partial \phi}{\partial y} = -\frac{2ed}{\hbar} B_x; \qquad (2)$$

$$\frac{\partial \phi}{\partial t} = \frac{2e}{\hbar} V,\tag{3}$$

where V is the junction voltage, t is time, ϕ is the order-parameter phase difference across the barrier, B_x and B_y are the x and y components of magnetic flux density \mathbf{B} in the barrier, and d is the sum of the London penetration depths (λ_1, λ_2) in the electrodes plus the thickness of the tunnel barrier t_{ay} .

Differentiating Eqs. (2) with respect to x and y, respectively, and replacing the z component of the Maxwell equation with the term for the displacement current written in terms of C_s (the capacitance per unit area),

$$\nabla \times \mathbf{B} = \mu_0 \left(\mathbf{j} + C_{\rm s} \frac{\partial V}{\partial t} \right) \tag{4}$$

vields

$$\frac{\partial^2 \phi}{\partial x^2} + \frac{\partial^2 \phi}{\partial y^2} = \frac{2ed}{\hbar} \mu_0 \left(j_z + C_s \frac{\partial V}{\partial t} \right). \tag{5}$$

Equations (1) and (3) can now be substituted for the terms on the right-hand side of Eq. (5) to give a single equation in ϕ

$$\frac{\partial^2 \phi}{\partial x^2} + \frac{\partial^2 \phi}{\partial y^2} - \frac{1}{v^2} \frac{\partial^2 \phi}{\partial t^2} = \frac{\sin \phi}{\lambda_1^2} , \qquad (6)$$

in which

$$\lambda_{\rm J} = (\hbar/2e\mu_0 dj_1)^{1/2} \tag{7}$$

and

$$v = 1/(\mu_0 C_c d)^{1/2} = c(t_{ox}/\epsilon d)^{1/2},$$
 (8)

where ϵ is the dielectric constant of the oxide, μ_0 is the permeability of a vacuum, and c is the velocity of light. The quantity λ_J has the dimension of length and describes the effective penetration distance of a magnetic field into the plane of the junction. The constant v represents a wave velocity and is typically $\approx c/25$.

In general terms, determination of the characteristic consists of solving Eq. (6) subject to the condition that the total junction gate current i_g is a maximum;

$$i_{g} = \int_{0}^{W} \int_{0}^{\ell} j_{1} \sin \phi \, dx dy. \tag{9}$$

It is relevant at this stage to give a brief description of the junction geometries that have been studied. This will be helpful in illustrating modifications required in Eqs. (6) and (9) for application to these particular cases.

The first and simplest structure is shown in plane and cross-sectional views in Fig. 1. The junction, consisting of the superconductors 1 and 2, separated by a thin oxide tunnel barrier ($t_{\rm ox} \approx 2$ -5 nm) is placed over a superconducting ground plane that provides magnetic shielding and serves to control the impedance of transmission lines used for interconnections. A third superconductor, the control line 3, is placed above and parallel to the junction to provide a magnetic field when a current i_c flows along it. Good magnetic coupling between the films is ensured by close spacing, obtained with thin oxides (SiO) that are vacuum-deposited on the ground plane and between electrodes 2 and 3.

This structure has already been used in one-dimensional analyses with constant W and j, [7]. Reference to

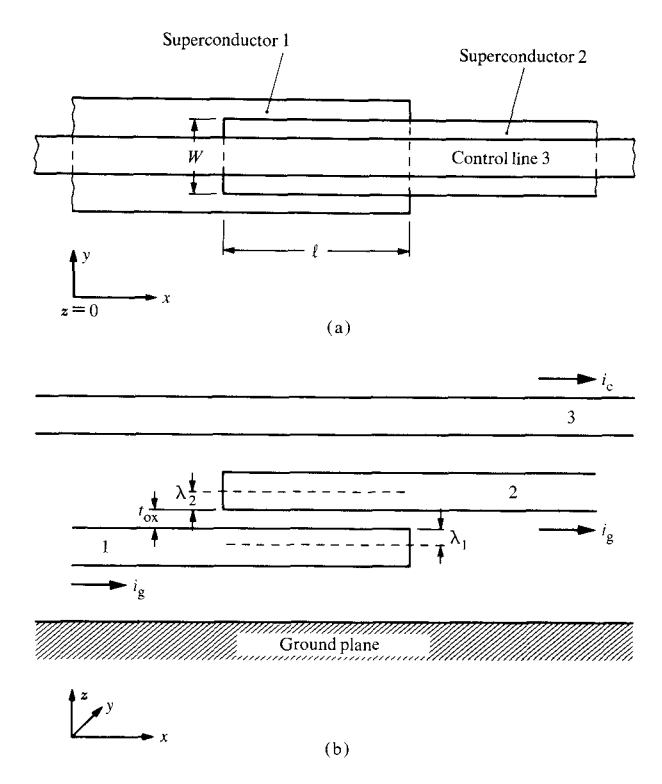


Figure 1 (a) Plane and (b) cross-sectional views of a simple inline Josephson junction showing the parameters that determine the characteristics.

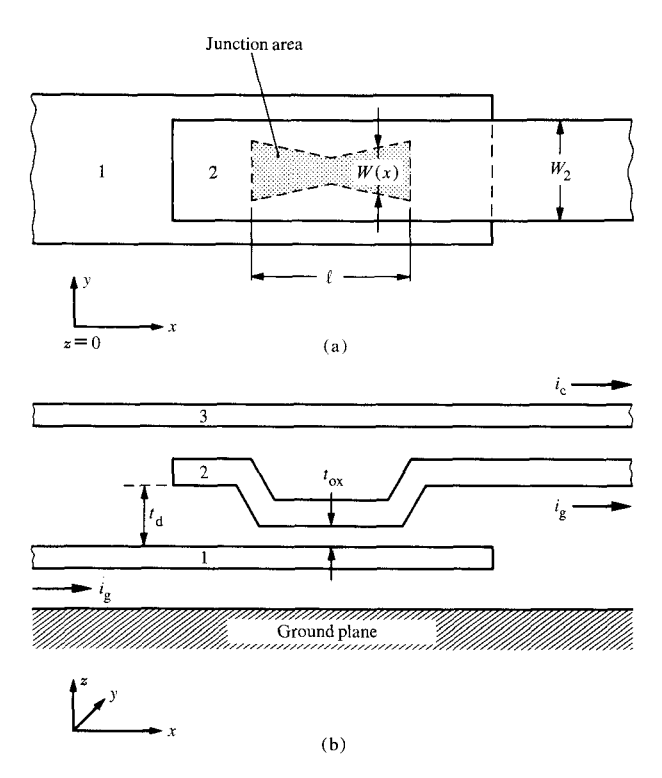


Figure 2 (a) Plane and (b) cross-sectional views of a "window" junction whose area is defined by an opening in a thin dielectric deposited between electrodes 1 and 2.

Eq. (2) shows that the absence of a magnetic flux density in the x direction (B_x) removes the y dependence of ϕ from Eq. (6). As mentioned in the introduction, j_1 can be made any arbitrary function of x without violating the one-dimensional condition. However, λ_1 is no longer constant and Eqs. (1), (2), (5), and (9) become

$$\frac{\partial^2 \phi}{\partial x^2} - \frac{1}{v^2} \frac{\partial^2 \phi}{\partial t^2} = \frac{2ed}{\hbar} \mu_0 j_1(x) \sin \phi$$
 (10)

and

$$i_{g} = W \int_{0}^{\ell} j_{1}(x) \sin \phi \, dx. \tag{11}$$

If W is varied instead of j_1 , the current flow is no longer everywhere parallel to the x axis and B_x is not generally zero. In this case, a one-dimensional treatment is an approximation in which Eqs. (10) and (11) are used to simulate a varying width. Computationally there is no difference between the two cases.

A varying junction width in the structure of Fig. 1 can be inconvenient with regard to the placement of the control line. A more favorable arrangement, especially when several control lines are required, is shown in Fig. 2. Here the top electrode 2 is of constant width W_2 and the junction area is surrounded by a vacuum-deposited oxide of thickness t_d greater than that of the tunnel barrier, as indicated in Fig. 2(b). In comparison with Fig. 1, the latter geometry provides greater freedom in varying the shape with less sacrifice in coupling efficiency k between the control lines and the junction. In addition, multiple-junction interferometers can also be designed on the same principle.

To analyze junctions of this geometry it is convenient to make the following substitutions. Noting that the inductance per unit length of the junction is $L = \mu_0 d/W$ and using Eq. (4) we can rewrite Eqs. (2) in the form

$$\frac{\partial \phi}{\partial x} = \frac{2\pi}{\Phi_0} L_x I_x; \qquad \frac{\partial \phi}{\partial y} = -\frac{2\pi}{\Phi_0} L_y I_y, \tag{12}$$

where I_x and I_y are the total surface currents flowing in the junction electrodes in the x and y directions. The inductances are not constant because of the thicker oxide outside the junction area. For example, in the case of L_x we must add two components in parallel: the inductance in the junction region $L_y = \mu_0 d/W$ and the inductance outside the junction $L_{\rm e} = \mu_0 (d + t_{\rm d} - t_{\rm ox})/(W_2 - W)$. Neglecting $t_{\rm ox}$ leads to

$$L_x = \frac{\mu_0 (d + t_d)}{W_2 + t_d W/d} \,. \tag{13}$$

This completes the summary of the principal relations re-

quired in the following section. More specialized formulae are derived in connection with specific models.

Numerical models and comparison with experiment

The three models to be described are based on two distinct approaches. Two are static models in which the phase difference ϕ yielding the maximum dc Josephson current is calculated directly from the one-dimensional, time-independent form of Eq. (6), or from a modification including a varying inductance L_x derived from Eqs. (12) and (13). The other models are based on an equivalent circuit representation using the general-purpose circuitanalysis program ASTAP [17]. This differs from the former models in that the junction is represented by an equivalent network of resistive, inductive, and capacitive elements to which a time-independent current ramp is applied. The characteristic is determined from the value of the current at which the junction switches to a finite voltage. More computer time is required with this approach but additional information is gained regarding the switching speed and the amplitude and voltage of junction resonances. The latter aspects are of considerable importance in circuit designs [18].

The junctions used in comparing experimental with calculated characteristics were based on the structure shown in Fig. 2. Oxidized Si wafers were used as substrates. A niobium ground plane was first evaporated onto the SiO₂, patterned by etching and, after growth of a thin anodic oxide (Nb₂O₅), was coated with 300 nm of SiO. Junction electrodes (1 and 2 in Fig. 2), consisting of Pb with small additions of In and Au, of thicknesses 200 and 350 nm, for base and counter electrodes, respectively, were patterned by photoresist and a lift-off technique. The junction area on the base electrode was delineated by an opening in a thin film (~200 nm) of SiO. Growth of the tunneling oxide was carried out in an rf plasma of oxygen with equipment and techniques similar to those first described by Greiner [19]. The junction electrodes were coated with about 500 nm of SiO to insulate them from the Pb-alloy control lines (one or more per junction) deposited on the oxide and lying parallel to the counter electrode. Various experiments established that the coupling factor k between the control lines and the junction was within the range 0.8-0.9, according to the particular geometry in use. The value is less than unity because of flux leakage caused by the finite width of the control lines and their small separation from the junction counter electrode.

• Constant junction width and varying current density
This model is described first because, although strictly
applicable only to junctions of constant width or inductance, it is relatively simple and yields a qualitative description of the characteristic for all shapes and values of

the ratio ℓ/λ_J . We use it here to outline the general behavior of the characteristic on either the current-density profile or shape before proceeding to more detailed models.

The calculation is based on a simple extension of the approach used in [7]. Assuming the junction to be of the geometry of Fig. 1 and of unit width we can define a current density $j_1(x)$ that varies along the x direction only. The mean current density is then

$$\bar{j}_1 = \frac{\bar{\lambda}_J}{\ell} \int_0^{\ell/\bar{\lambda}_J} j_1(x) dx \tag{14}$$

and the mean penetration depth can be defined by

$$\bar{\lambda}_{i} = (\Phi_{o}/2\pi\mu_{o}d\bar{j}_{i})^{1/2}.$$
(15)

For comparison of the characteristics obtained from various current-density profiles, it is convenient to use dimensionless units. Expressing the x coordinate in units of $\bar{\lambda}_{J}$, and applying Eq. (6) to the one-dimensional time-independent case, we obtain the simple equation

$$\frac{\partial^2 \phi}{\partial x^2} = J \sin \phi, \tag{16}$$

where $J = j_1(x)/\overline{j_1}$. The normalized gate and control currents, per unit junction width, are given by

$$I_{\rm g} = \frac{i_{\rm g}}{\hat{\lambda}_{\rm J} \hat{J}_{\rm l}} = \int_{\rm c}^{\epsilon/\hat{\lambda}_{\rm J}} J \sin \phi \, dx \tag{17}$$

and

$$I_{\rm c} \equiv \frac{i_{\rm c}}{\tilde{\lambda}_{\rm j} \tilde{J}_{\rm i}} \ . \tag{18}$$

The boundary conditions for $\partial \phi/\partial x$ at x=0 and $\ell/\bar{\lambda}_J$ are easily determined from Fig. 1(b), where it is seen that the presence of the ground plane causes all junction current to flow on the underside of electrode 1 at x=0. Hence, from Eqs. (2) [noting that $B_y=\mu_0 I_x$] and (15),

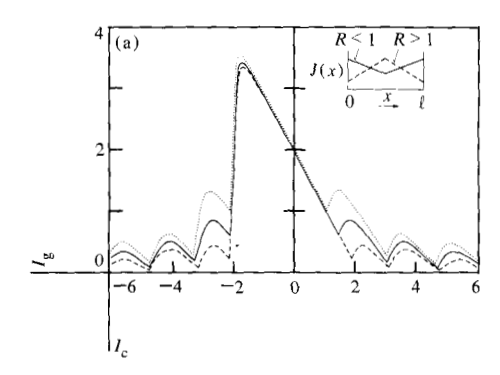
$$\left. \frac{\partial \phi}{\partial x} \right|_{0} = I_{c}. \tag{19}$$

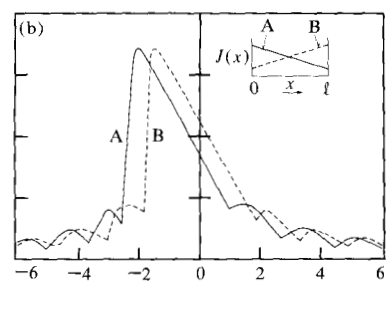
At $x = \ell/\bar{\lambda}_{\rm J}$, the entire junction current contributes to the magnetic flux density $B_{\rm u}$, giving

$$\left. \frac{\partial \phi}{\partial x} \right|_{\ell i \tilde{\lambda}_{1}} = I_{c} + I_{g}. \tag{20}$$

This choice of geometry allows Eq. (16) to be treated as an initial-value problem since the unknown $I_{\rm g}$ does not appear in the boundary condition (19). With this approach, condition (20) is unnecessary; however, it serves as a useful check on the accuracy of the computation because the solution of Eq. (16) also yields $\partial \phi/\partial x$ at $x = \ell/\bar{\lambda}_{\rm J}$. The value of $I_{\rm g}$ calculated from the insertion of $\partial \phi/\partial x$ at $x = \ell/\bar{\lambda}_{\rm J}$ in Eq. (20) can then be compared with that obtained from Eq. (17).

181





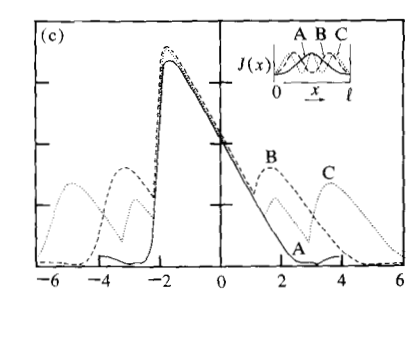


Figure 3 (a) Calculated characteristics showing the effect of increasing (dotted curve; R=0.5) or decreasing (dashed curve; R=2) the current density at the ends of the junction. The continuous line for a uniform current density (R=1) is shown for comparison; $\ell/\lambda_J=4$. (b) The influence of an asymmetric current-density distribution; $\ell/\bar{\lambda}_J=4$, $R'=J_{\rm max}/J_{\rm min}=4$. (c) The characteristics of junctions having a sinusoidal current density distribution with minima at the ends of the junction. The number of maxima in J are 1 (Curve A), 2 (Curve B), and 3 (Curve C); $\ell/\bar{\lambda}_J=4$, R'=4.

It is important to note that structures of the forms of Figs. 1 and 2 always lead to characteristics that are asymmetric about the axis $i_{\rm g}=0$. Symmetric curves are obtained by other geometries, such as feeding the current $i_{\rm g}$ to both ends of the counter electrode. In this case the characteristic can be obtained from the asymmetric case simply by using the shear transformation

$$i_{cs} = i_c + i_g/2,$$
 (21)

applied to the i_c axis only.

The solution of Eq. (16) for constant J, leading to the determination of I_g , has been described in [7]; only brief details need be given here. Since ϕ_0 , the phase difference at x = 0, is undefined, Eqs. (16) and (17), with the starting condition (19), were solved numerically for a number of values (generally 62) of ϕ_0 between 0 and 2π by using a simple integration routine [20] for Eq. (16) and 20 intervals in x. The value of ϕ_0 corresponding to the maximum value of I_{α} was then found and the process repeated for smaller steps in ϕ_0 around the initial solution. The difference in I_a determined from Eqs. (17) and the boundary condition (20) was generally less than 1%, provided a smoothly varying function was used for J. The method used to determine ϕ_0 was satisfactory for $\ell/\tilde{\lambda}_1 \leq 8$. This procedure yields the envelope of the characteristic. Although not generally carried out in the following treatments, it is a relatively easy matter to determine vortexmode boundaries which lie below the envelope by seeking all the positive maxima in the solutions of i_g versus ϕ_0 . Written in FORTRAN IV, the program took about one minute of CPU time to calculate a complete characteristic of 50-80 points, using a high-speed, 3M-byte computer.

Figures 3(a-c) illustrate the results obtained from several simple current density profiles and a fixed $\ell/\tilde{\lambda}_1 = 4$.

Figure 3(a) is chosen to show the influence of increasing or decreasing J at the ends of the junction relative to the center, using a linear profile as sketched in the insert. The ratio R is here defined by the ratio of J at $x = \ell/2\bar{\lambda}_J$ to J at x = 0. The side lobes are rather sensitive to R, increasing in amplitude when J has maxima at the ends of the junction and decreasing when its maximum is in the center. In contrast, the central lobe is relatively independent of the profile; the small increase (decrease) in I_R at the maximum for R < 1 (R > 1) can be understood from the current distribution within the junction, which is concentrated near the ends [3-6] at the corresponding value of I_C .

The effect of asymmetry in J about the center point of the junction $(x=\ell/2\tilde{\lambda}_J)$ is illustrated in Fig. 3(b), again for a linear variation in J. Here, we define a ratio $R'\equiv J_{\max}/J_{\min}$; in this case, R'=4. Two basic features are apparent. First, there is a displacement of the center lobe to the left or right depending on whether the maximum in J is at x=0 or $x=\ell/\tilde{\lambda}_J$, respectively. Second, the maximum amplitudes of the pairs of equal-order vortex modes for positive and negative values of I_c are no longer equal. Thus, application of the transformation for symmetric current feed, Eq. (21), here does not lead to a symmetric characteristic. However, in Fig. 3(b) it may be noted that curve A maps onto curve B with the transformation $I'_c = -(I_c + I_g)$.

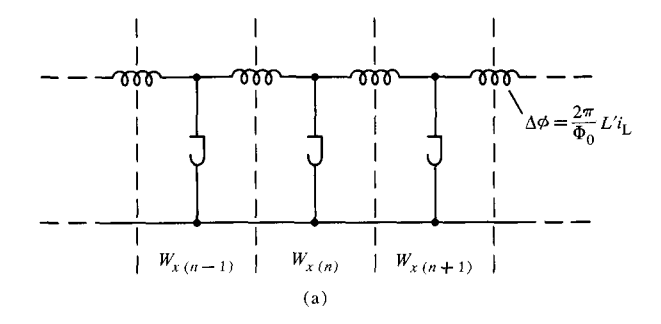
Figure 3(c) shows the effect of several maxima in J, in this instance with a cosine distribution and R' = 4. Curves A, B, and C were obtained with $J = 1 + [(R'-1)/(R'+1)] \cos [\pi(1+2mx\tilde{\lambda}_3/\ell)]$ with m (representing the number of maxima in J) = 1, 2, and 3, respectively. This function has J minima at the ends of the junction, and the n = 1, 2, and 3 vortex modes are almost entirely suppressed for m = 1, 2, and 3, respectively.

The foregoing results can be applied in two ways: to calculate the characteristic obtained from a given current density or width profile, and, by reversing the sequence, to make an estimate of the $j_1(x)$ leading to a given measured characteristic. In the former case, the junction width W(x) is the parameter of interest since j, cannot be varied easily in a reproducible manner over the area of a single junction and is, therefore, usually assumed to be constant in designing junctions with specific characteristics. However, a number of factors can lead to a spatially varying current density; e.g., a) microshorts, b) different crystal orientations of a polycrystalline base electrode having slightly varying oxide growth rates, and c) back-sputtered material from areas surrounding the junction for tunneling oxides grown in an rf plasma [19] (local influence on oxide thickness).

A systematic variation in j_1 (case c) is generally of more interest than the random variations (cases a and b). Where $j_1(x)$ is likely to be smoothly varying with maxima or minima limited to one or two, the model is capable of yielding a reasonably unambiguous interpretation of the current-density profile. For example, the relative amplitude of the n=1 vortex modes indicates whether j_1 has a maximum or a minimum at the ends of the junction [Fig. 3(a)]. For more complex profiles, however, the results must be regarded with caution because they may not be a unique solution to the measured characteristic [16]. This model has been found useful for qualitative investigations where its high speed of execution allows many characteristics to be obtained in a short time.

• Time-dependent circuit model (dynamic simulation) Some circuit applications require Josephson junctions having a very small dc Josephson gate current, $i_{\rm g}(i_{\rm c})/i_{\rm g}(0)$, at modest values of the control current $i_{\rm c} \geq i_{\rm c}(0)$ [15]. It has been indicated in the previous section that junctions having a reduced width at the ends may satisfy this requirement. In addition, for the circuits of [15], a knowledge of the dynamic (switching) behavior of the junctions is of importance in order to estimate the switching delays and the influence of internal junction resonances [18] thereon. Consequently, although only the static behavior is considered here, the following models are based on the full time-dependent equations applied to junctions of the form of Fig. 2.

The circuit-analysis program used here was ASTAP[17], in which a lumped representation of the terms in the equations is obtained with current sources, capacitors, and inductors. These elemental values are derived from the equations of the preceding section in the following manner.



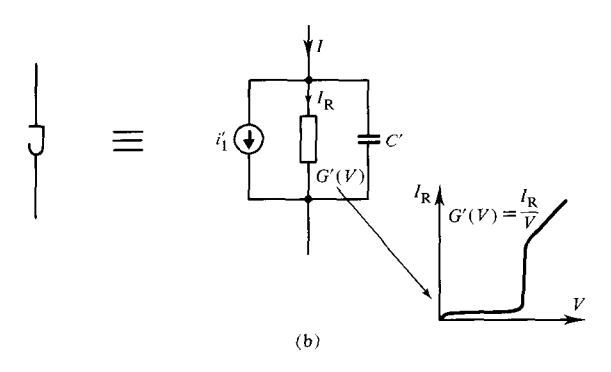


Figure 4 Equivalent-circuit models of a Josephson junction. (a) Distributed-junction model with a point junction as sectional element (b) in which $i_1' = \text{Josephson current}$, G'(V) = single-particle contribution, and C' = capacitance of the point junction.

Assuming a magnetic field in the y direction to obtain a one-dimensional approximation, Eq. (5) becomes

$$\frac{\Phi_0}{2\pi d} \frac{d^2 \phi}{dx^2} = \mu_0 \left[j_1 \sin \phi + V G_s(V) + C_s \frac{\partial V}{\partial t} \right], \tag{22}$$

where the additional term $VG_{\rm s}(V)$ represents the contribution of the single-particle current per unit area, and V is the junction voltage. Eliminating the second derivative of ϕ with Eq. (3) yields

$$\left[\frac{1}{d\mu_0} \frac{\partial^2}{\partial x^2} - C_s \frac{\partial^2}{\partial t^2} - G_s(V) \frac{\partial}{\partial t}\right] V = j_1 \frac{2\pi}{\Phi_0} V \cos \phi. \quad (23)$$

To obtain the characteristic for shaped window junctions, the width W has to be made x-dependent, leading to a sectioned model in the x direction. With W(x), we can now obtain the element values per unit length of the distributed model by comparison of Eqs. (23) with the expression for a transmission line, namely,

$$\left(\frac{1}{L'}\frac{\partial^2}{\partial x^2} - C'\frac{\partial^2}{\partial t^2} - G'\frac{\partial}{\partial t}\right)V = i'_1\frac{\partial\phi}{\partial t}\cos\phi, \qquad (24)$$

leading to $C' = C_s W(x)$, $G' = G_s(V)W(x)$, $i_1' = j_1 W(x)$ and, according to Eq. (13), $L' = \mu_0 (d - t_d)/(W_2 + t_d W/d)$.

Figure 4(a) shows the elements of the distributed junction model in which each section is represented by a

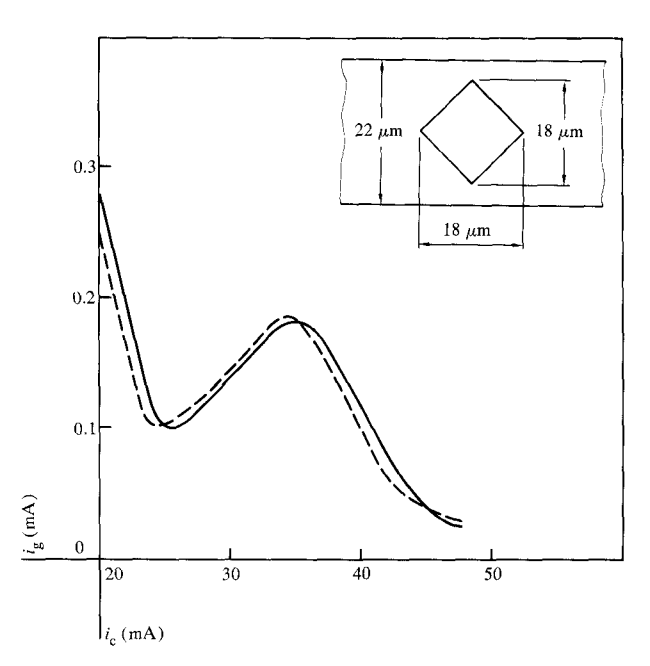


Figure 5 Simulated (--) and measured (-) gain characteristics of a diamond-shaped Josephson junction in the vicinity of the first null in i_g . For the simulation, the equivalent-circuit model of Fig. 4 has been used.

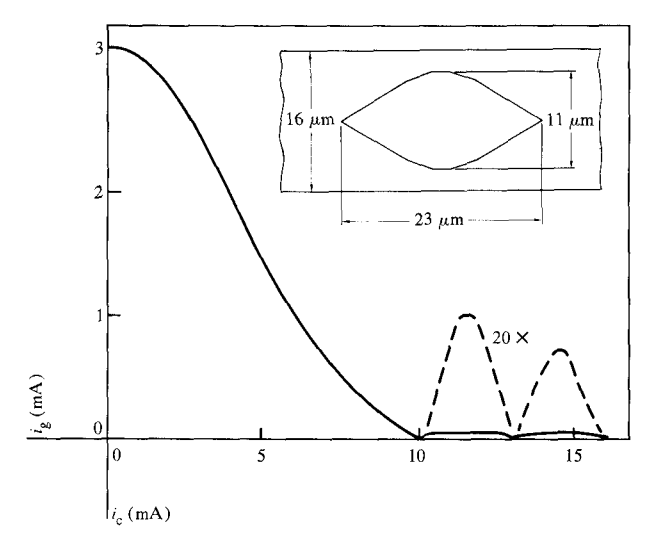


Figure 6 Computed threshold characteristic of the junction with an approximated sine shape; $j_1=2.2~\mathrm{kA/cm^2},~\ell/\lambda_\mathrm{J}\approx2.5.$

''point'' junction of length $\ell' << \lambda_J$ as shown in Fig. 4(b). In this figure the following equalities hold:

$$i_{\rm J}'=i_{\rm 1}'\sin\phi,$$

$$\dot{\phi} = V \frac{2\pi}{\Phi_0} ,$$

$$I = i'_1 \sin \phi + \frac{\Phi_0}{2\pi} G'(V) \dot{\phi} + C' \frac{\Phi_0}{2\pi} \ddot{\phi}.$$

Figure 5 illustrates the experimental characteristic (—) of a diamond-shaped junction in the vicinity of the first null in $i_{\rm g}$, in comparison with calculations (——), where $j_1=2.3~{\rm kA/cm^2}$. Evidently, agreement between experiment and the model is fairly good.

This model has been used to calculate junction shapes yielding the maximum side-lobe suppression. Simulations with shapes of the form $\sin (\pi x/\ell)$, $\sin^2 (\pi x/\ell)$, and a circle, have shown that the choice of $\sin (\pi x/\ell)$ minimizes the side lobes [21]. An example of the characteristic computed for such a junction having an approximated sine shape is shown in Fig. 6. For $i_c \ge 10$ mA, $j_1 = 2.2$ kA/cm², and $\ell/\lambda_J = 2.5$, the maximum value of the dc Josephson gate current i_g is less than two percent of its value at $i_c = 0$. This is a significant side-lobe suppression in comparison with the diamond-shaped junction of Fig. 5.

It is appropriate to mention at this point that the ASTAP simulation for each point of the characteristic is obtained by increasing the junction current from zero in small increments, and solving the equations for each current. The current at which a finite voltage first appears across the junction is then taken as the $i_{\rm g}$ for the previously defined value of $i_{\rm c}$. The accuracy of the solutions thus depends on the size of the current increments and (to be shown) on the number of sections. The solutions are continued above the point at which the junction switches to a voltage state, thus yielding information on the *time* taken for the voltage to build up to its maximum value, the gap voltage $2\Delta/e$ (or $V_{\rm g}$). The behavior in the voltage regime yields information on switching speed and the influence of junction resonances.

The junction of Fig. 6 has a fairly small value of the ratio $\ell/\lambda_{\rm J}$ (≈ 2.5) and has therefore almost symmetric characteristics about $i_{\rm c}=0$. In some circuit applications a strongly asymmetric characteristic is required, implying a larger $\ell/\lambda_{\rm J}$ ratio [15]. With the model considered in this section the magnetic field caused by the junction current is automatically included so that no modifications, except an increase in the number of sections, are required for large $\ell/\lambda_{\rm J}$ ratios.

Figure 7(a) shows that good side-lobe suppression is also obtained in long junctions (i.e., $\ell/\lambda_{\rm J}\approx 6$) with a sinusoidal shape. Apart from the scaling factor for $i_{\rm c}$, caused by a nonunitary coupling factor ($k\approx 0.82$), there is excellent agreement between calculated (——) and measured (—) characteristics in the experimental junction when 60 sections are used ($\ell'\approx 0.1\lambda_{\rm J}$) for the simulation [see Fig. 7(b)]. For Fig. 7(a), $j_{\rm I}=1.6~{\rm kA/cm}^2$.

In order to investigate the accuracy and validity of the one-dimensional model, a two-dimensional distributed equivalent circuit has been studied. A total of 196 elements (14 × 14) was used to represent a diamond-shaped junction of length $\ell/\lambda_{\rm J}\approx 1.5$. In comparison with the one-dimensional approximation, the central lobe was essentially unchanged and only small deviations (maximum of $\approx 20\%$) were observed in the side lobes. Thus, for the shapes studied, the one-dimensional model is adequate for most purposes, an important finding in view of the very long computation time required for the two-dimensional model. In fact, the computation time is not trivial even for the one-dimensional case; one point of the characteristic of a 60-section junction requires about 30 min of CPU time on our computer.

• Static model for varying inductance

This last model is similar to the one first described, involving constant W and varying j_1 . However, it applies to structures having varying inductance along the length ℓ and constant j_1 (Fig. 2). Although restricted to the static characteristics, the computation time is much less than that required by ASTAP. In this respect, it is advantageous for preliminary investigations of junction characteristics, such as determination of the optimum shape and dimensions consistent with the tolerances imposed by a given circuit.

Again, we restrict the analysis to one dimension. Incorporation of an x-dependent inductance into a time-independent form of Eq. (5) is easily obtained by differentiating the x component of Eq. (12) with respect to x and noting that $\partial i/\partial x = j_i W \sin \phi$, leading to

$$\frac{\partial^2 \phi}{\partial x^2} = \frac{\partial L}{\partial x} \frac{1}{L} \frac{\partial \phi}{\partial x} + \frac{2\pi}{\Phi_0} L j_1 W \sin \phi, \qquad (25)$$

with L given by Eq. (13). In the calculations W_2 was assumed to be constant along the length but, in principle, it can also be x-dependent.

The junction current is given by a relation similar to Eq. (11):

$$i_{g} = j_{1} \int_{0}^{\epsilon} W \sin \phi \, dx \,, \tag{26}$$

and the boundary conditions are

$$\left. \frac{\partial \phi}{\partial x} \right|_{0} = \left. \frac{2\pi}{\Phi_{0}} L(0) i_{c}; \right. \tag{27}$$

$$\frac{\partial \phi}{\partial x}\bigg|_{\ell} = \frac{2\pi}{\Phi_0} L(\ell) (i_c + i_g). \tag{28}$$

The solution of Eqs. (25)-(28) followed the same procedure used in the section on constant W and varying j_1

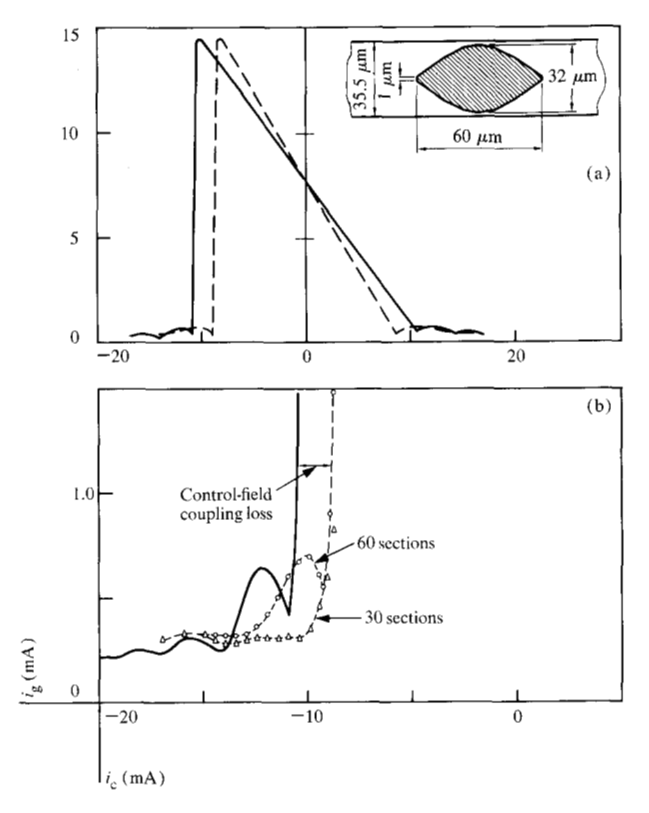


Figure 7 Measured (—) and computed (——) threshold characteristics of the sine-shaped junction shown; $(\ell/\lambda_J \approx 6)$, $j_1 = 1.6 \text{ kA/cm}^2$. (a) Full characteristic and (b) computed characteristic for $i_c > i_c(0)$, using the distributed model with 30 (\triangle) and 60 (\bigcirc) sections.

with the difference that a Runge-Kutta routine was used to integrate Eq. (25). Since the model was mainly devoted to the calculation of specific geometries, real quantities were used in place of the dimensionless values used in the first model.

The program was written in FORTRAN IV. For the solution of Eq. (25), twenty integration steps were found to give results accurate to about 2%, adequate for most purposes. In this case, each point took less than one second to compute; a complete characteristic could be obtained in ≈ 1 min.

Applied to sinusoidal junctions, such as that shown in Fig. 7(a), the results were the same as those obtained by ASTAP simulation to $\pm 2\%$. A further extension of the model is of interest: its application to some types of interferometers having two or more junctions. The characteristics of such devices, based on point junctions, have been determined by a number of methods [22, 23]. In some cases, however, the junctions cannot be regarded as point devices $(\ell/\lambda_{\rm J} \geq 1)$ and it is desirable to include the

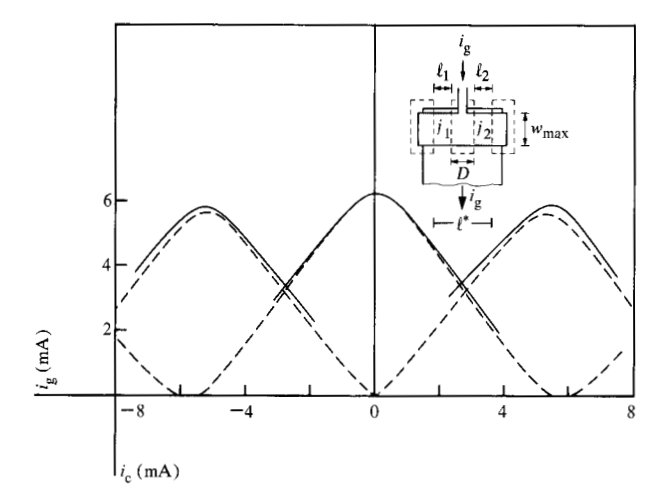


Figure 8 Calculated (——) and experimental characteristics (—) of the interferometer shown. In the calculation, $j_1 = 2.4 \text{ kA/cm}^2$, $d = 0.18 \mu\text{m}$, and $t_d = 0.2 \mu\text{m}$. The experimental values of i_p are multiplied by k = 0.80.

influence of the finite length. An example is the singleflux-quantum (SFQ) memory cell [13, 14]. The geometry and experimental characteristic of a simple version of such a cell are shown in Fig. 8. Here, the finite junction length results in a reduction in the amplitude of the side lobes in comparison to the central lobe. To calculate (see dashed lines in figure) the characteristic with the present model it is only necessary to approximate the two separate junctions by a single junction to preserve the continuity of Eq. (25). This may be done by connecting the two junctions with a narrow filament and by providing a graded region between the junctions proper (of width w_{max}) and the filament to avoid discontinuities. The width of the filament w_{\min} can be made arbitrarily small so that it contributes negligible gate current. A suitable function for junction width W in the region $0 \le x \le \ell^*/2$, used in the calculation of the interferometer of Fig. 8, is

$$W = w_{\min} + \frac{w_{\max} - w_{\min}}{1 + (2x/a\ell^*)^n}$$
 (29)

 $(d = 0.18 \ \mu\text{m}, \ t_{\rm d} = 0.2 \ \mu\text{m}, \ \text{and} \ j_1 = 2.4 \ \text{kA/cm}^2)$. The values were $w_{\rm min} = 0.01 \ \mu\text{m}, \ w_{\rm max} = 17.8 \ \mu\text{m}, \ n = 20,$ and $a = \ell/(\ell^*/2) = 7.43/12.76 = 0.58$, where $\ell^* = \ell_1 + \ell_2 + D \ (\ell_1 = \ell_2 = 7.43 \ \mu\text{m}, \ D = 10.65 \ \mu\text{m}$; see inset). Because of the fairly abrupt change in W at $x \approx \ell$ the number of integration steps was increased to 40.

It will be seen from the inset of Fig. 8 that the current feed to the interferometer is symmetric; hence, the calculated curves were modified for this condition by applying the shear transformation, Eq. (21).

With the inclusion of an assumed coupling factor k=0.8 for the experimental data, the agreement between the experimental (—) and calculated (——) curves is quite good. In particular, the effect of finite junction length on the amplitude of the side lobes ("control effect") is rather well described by the model. The small deviations between theory and experiment most likely result from small asymmetries in j_1 and the geometry, and from two-dimensional effects.

The model may also be extended to three-junction interferometers having geometries similar to that of Fig. 8.

Summary

In cryogenic circuits based on Josephson junctions, the static characteristic of the junction determines the regions of switching. Different circuits require different characteristics. For example, overlapping vortex modes are required in single-flux-quantum memory cells, whereas some types of logic gate demand that $i_{\rm g}$ be reduced to less than 2% of its maximum value with relatively small control currents $i_{\rm c}$. The former case is satisfied by two-junction interferometers and the latter by sinusoidally shaped junctions having maximum widths in the center. For these applications it is essential to be able to calculate the characteristic, both static and dynamic, for given geometry and electrical parameters, first, to obtain the most suitable shape and second, to derive the operating currents and their tolerances.

To make the problem manageable, while at the same time obtaining reliable results that are in good agreement with experiment, a number of simplifications and details have been investigated and tested against device measurements. The principal findings on the static characteristics are summarized here:

- Most shaped junctions or interferometers have part or all of the junction defined by a relatively thick insulating film, which isolates the electrodes outside of the required junction area. For electrodes of constant width this results in a varying inductance along the junction length, which significantly influences the characteristics and which must be included in the theory.
- Consideration of the phase difference φ along the length of the junction only, assuming invariance over the width, greatly simplifies the calculations by reducing them to one dimension. The validity of the one-dimensional treatment, in cases where the gate current flows predominantly along the length of the junction, has been tested theoretically and experimentally.

Static solutions based on numerical integration of the differential equation describing $\phi(x)$ have the advantage

of speed, whereas the computationally longer dynamic simulation has the advantage of yielding information on both the resonance behavior and the static characteristics.

It has been demonstrated that the one-dimensional approximation, including the variation of inductance along the length, gives a rather good description of the characteristics of a wide range of junction shapes and interferometers. The models described have been used successfully in designing gates for the logic circuits of a cross-sectional model for a 16K-bit SFQ memory [24].

Acknowledgments

The authors are indebted to P. Wolf for much helpful guidance, to P. Guéret for kindly providing the interferometer data, and to W. Heuberger for fabricating the devices.

References

- 1. J. M. Rowell, Phys. Rev. Lett. 11, 200 (1963).
- 2. M. D. Fiske and I. Giaever, Proc. IEEE 52, 1155 (1964).
- 3. C. S. Owen and D. J. Scalapino, *Phys. Rev.* **164**, 538 (1967).
- 4. J. Matisoo, J. Appl. Phys. 40, 1813 (1969).
- 5. K. Schwidtal, Phys. Rev. B 2, 2526 (1970).
- D. L. Stuehm and C. W. Wilmsen, J. Appl. Phys. 45, 429 (1974).
- 7. S. Basavaiah and R. F. Broom, *IEEE Trans. Magnetics* MAG-11, 759 (1975).
- A. Barone, W. J. Johnson, and R. Vaglio, J. Appl. Phys. 46, 3628 (1975).
- R. F. Broom, R. Jaggi, R. B. Laibowitz, Th. O. Mohr, and W. Walter, Proceedings of the 14th International Conference on Low Temperature Physics (LT 14), Otaniemi, Finland, M. Krusius and M. Vuoro, Eds., North-Holland Publishing Co., Amsterdam, 1975, ch. 4, p. 172.

- 10. J. Matisoo, Proc. IEEE 55, 172 (1967).
- 11. W. Anacker, IEEE Trans. Magnetics MAG-5, 968 (1969).
- W. Anacker, in Solid-State Devices 1976, R. Müller and E. Lange, Eds., Institute of Physics, Conference Series Number 32 (Bristol and London, 1977). Invited paper at the 6th European Solid-State Device Research Conference (ESSDERC), Technische Universität München, BRD, September 13-16, 1976.
- H. Zappe, Appl. Phys. Lett. 25, 424 (1974); P. Guéret, Appl. Phys. Lett. 25, 426 (1974).
- 14. P. Guéret, Th. O. Mohr, and P. Wolf, IEEE Trans. Magnetics MAG-13, 52 (1977).
- 15. A. Moser, IEEE J. Solid-State Circuits SC-14, 672 (1979).
- 16. H. H. Zappe, Phys. Rev. B 11, 2535 (1975).
- IBM Advanced Statistical Analysis Program, IBM Publication No. SH20-1118, available through IBM branch offices.
- R. E. Eck, D. J. Scalapino, and B. N. Taylor, *Phys. Rev. Lett.* 13, 15 (1964).
- 19. J. H. Greiner, J. Appl. Phys. 42, 5151 (1971).
- 20. R. de Vogelaire, J. Res. NBS 54, 119 (1955).
- 21. W. Kotyczka, unpublished results.
- 22. B. S. Landman, IEEE Trans. Magnetics MAG-13, 871 (1976).
- E. O. Schulz-DuBois and P. Wolf, Appl. Phys. 16, 317 (1978).
- R. F. Broom, P. Guéret, W. Kotyczka, Th. O. Mohr, A. Moser, A. Oosenbrug and P. Wolf, *IEEE J. Solid-State Circuits* SC-14, 690 (1979).

Received March 19, 1979; revised October 3, 1979

R. F. Broom and A. Moser are located at the IBM Zurich Research Laboratory, 8803 Rüschlikon-ZH, Switzerland; W. Kotyczka is now with Stäfa Control System AG, 8712 Stäfa-ZH, Switzerland.